

# Influence of Deleterious Phases Precipitation in the Corrosion Resistance Measured by Double Loop Electrochemical Polarization Reactivation Test in Superduplex Stainless Steel

Juan Manuel Pardal<sup>a\*</sup>, Sérgio Souto Maior Tavares<sup>a</sup>, Guttemberg Chagas de Souza<sup>a</sup>,

Maria da Penha Cindra Fonseca<sup>a</sup>, Eduardo Ariel Ponzio<sup>b</sup>, Marcelo Camargo Severo de Macedo<sup>c</sup>

<sup>a</sup>Programas de Pós-Graduação em Engenharia Mecânica (PGMEC) e Montagem Industrial, Universidade Federal Fluminense – UFF, Rua Passo da Pátria, 156, CEP 24210-240, Niterói, RJ, Brazil

<sup>b</sup>Programa de Pós-Graduação em Química, Departamento de Físico-Química, Universidade Federal Fluminense – UFF, Rua Outeiro de São João Batista, s/n, CEP 24020-141, Niterói, RJ, Brazil

<sup>c</sup>Programa de Pós-Graduação em Engenharia Mecânica, Departamento de Engenharia Mecânica, Universidade Federal do Espírito Santo – UFES, Rua Av. Fernando Ferrari, s/n, CEP 29060-970, Vitória, ES, Brazil

Received: April 3, 2015; Revised: June 4, 2015

This work investigates the influence of deleterious phases precipitation on the corrosion resistance of two wrought superduplex stainless steels UNS S32750 with similar composition, but different grain sizes. Isothermal treatments were carried out to introduce different amounts of deleterious phases, such as chi ( $\chi$ ), sigma ( $\sigma$ ) and secondary austenite ( $\gamma_2$ ). The specimens were tested by double loop electrochemical potentiodynamic reactivation test (DL-EPR). The kinetics of precipitation in the two steels was different due to the difference of the grain sizes. The results show a correlation between the sensitization degrees, measured by DL-EPR, with the amount of deleterious phases precipitated.

**Keywords:** *superduplex stainless steel, deleterious phases precipitation, corrosion resistance, DL-EPR tests*

## 1. Introduction

Duplex (DSS) and superduplex stainless steels (SDSS) are materials used extensively in petrochemical industries due to elevated mechanical strength and high pitting corrosion resistance<sup>1</sup>. These characteristics are attributed to microstructural features, such as; grain refinement, approximately equal parts of austenite ( $\gamma$ ) and ferrite ( $\delta$ ), and also to the alloying elements Cr, Mo and N dissolved in these phases<sup>2</sup>. However, during welding, heat treatment and hot forming operations, deleterious phase precipitation may compromise the use of these materials in severe service conditions.

The most dangerous and also the most studied intermetallic compound in austenitic-ferritic stainless steels is the sigma phase ( $\sigma$ ), which can be formed by slow continuous cooling<sup>3,4</sup> or by isothermal treatments<sup>5</sup>. According to published Temperature-Time-Transformation (TTT) diagrams<sup>1,6</sup>, the higher kinetics of precipitation occurs in the 800 – 950 °C range. Ferrite former elements, such as Cr, Mo and Si, increase the susceptibility of sigma phase formation in DSS and SDSS. Secondary austenite ( $\gamma_2$ ) can also be formed during thermal treatments. The precipitation can occur at ferrite/ferrite grain boundaries, as chromium nitrides particles, in association to sigma phase as divorced eutectoid ( $\delta \rightarrow \gamma_2 + \sigma$ ), or even due to the growing of primary austenite<sup>7,8</sup>.

Besides  $\gamma_2$  and  $\sigma$ , the chi phase ( $\chi$ ) may also be formed in Mo containing steels heated in the 700 – 900 °C range<sup>9,10</sup>.

Although all these phases may cause the decrease of mechanical properties and corrosion resistance,  $\sigma$  may be considered the most dangerous. The kinetics of precipitation of deleterious compounds is a function of the chemical composition<sup>11</sup> and grain size<sup>5</sup>.

For the reasons explained above, it is very important to characterize DSS and SDSS by electrochemical techniques to determinate the degree of sensitization and hence the susceptibility of deleterious phases precipitation. Nowadays one of the most employed techniques is the double loop electrochemical polarization reactivation test (DL-EPR). The development and optimization of a procedure based around this technique for assessing sensitization degree in DSS and SDSS is therefore of great interest. Generally for DSS, the electrolyte used is sulphuric acid ( $H_2SO_4$ ), with the increase of KSCN and NaCl additions. Lopez et al.<sup>12,13</sup> analyzed the influence of  $\sigma$  phase precipitation on corrosion resistance in a DSS UNS31803 sample aged at 675 °C and 900 °C by DL-EPR testing using a 2.00 M  $H_2SO_4$  + 0.01 M KSCN + 0.50 M NaCl solution at 30 °C. These authors considered the material susceptible to intergranular corrosion when the degree of sensitization ( $DOS = I_T/I_a$ ) was greater than 0.05<sup>12,13</sup>.

However, other researches<sup>14,15</sup> were performed using different concentrations of HCl, taking into account the temperature effect. For instance, Amadou et al.<sup>14</sup>, evaluated the sensitization of UNS S31250 duplex stainless steels

\*e-mail: juanpardal@vm.uff.br

(DSS) by using a solution with 33%  $H_2SO_4$  + 0.3% HCl, at room temperature. These tests were performed at a potential scan rate of  $2.5 \text{ mV s}^{-1}$ . Recently, Deng et al.<sup>15</sup>, demonstrated that the modified DL-EPR measurement, using a solution of 33%  $H_2SO_4$  + 0.1% HCl at 20 °C and scan rate of  $2.5 \text{ mV s}^{-1}$ , could successfully characterize the interactions between precipitation, chromium depletion and intergranular corrosion with high sensitivity and reproducibility of lean DSS 2101. Hong et al.<sup>16</sup> indicates that the optimum DL-EPR condition to evaluate sensitization degree (DOS) of SDSS UNS S32750 is in a 2 M  $H_2SO_4$  + 1.5 M HCl solution with a scanning rate of  $1.5 \text{ mV s}^{-1}$  at a temperature of 30 °C.

Other researches were performed by continuous cooling in order to simulated heat affected zone in weld joints. Yang et al.<sup>17</sup> studied the microstructure and corrosion behavior by DL-EPR in the simulated heat affected zone of 2205 DSS by using a thermo-mechanical simulator. Pardal et al.<sup>3</sup> analyzed the DOS behaviour in specimens of 2505 SDSS obtained by different continuous cooling treatments. Both researches were performed using the same solution proposed by Lopez et al.<sup>12,13</sup> using a scan rate of  $1 \text{ mV s}^{-1}$ .

The purposes of this work were, in the first instance, to determinate the best temperature at which the premature deleterious phases precipitation can be detected, by using the DL-EPR technique with a 2.00 M  $H_2SO_4$  + 0.01 M KSCN + 0.50 M NaCl solution with a sweep rate of  $1.0 \text{ mV.s}^{-1}$ ; secondly, to determine a correlation of deleterious phases precipitation by DL-EPR testing and optical microscopy analysis in specimens that were isothermally heat treated. Also of interest was the comparative analysis of two SDSS with similar chemical compositions, but different grain sizes.

## 2. Experimental

The compositions of the two materials studied are shown in Table 1. SD-A and SD-B have similar chemical compositions, both fitting the UNS S32750 specification. Austenitic and ferritic volumetric fraction and grain sizes of each material are shown in Table 2. The volume fractions of phases were measured by image analysis of the specimens prepared with Beraha's reagent (100 ml  $H_2O$  + 20 ml HCl + 0.3 - 0.6 g potassium metabissulfite), and grain sizes were determined by electron backscattered scanning diffraction (EBSD), as reported in a previous work<sup>5</sup>. SD-A and SD-B

have different grain sizes because they were processed by different ways. The SD-A (fine grained) was cut from a hot rolled and solution treated sheet with 9.5 mm thickness. The SD-B specimen was cut from a forged and solution treated bar with 203 mm of diameter. The hot forging resulted in a much coarser grain size of ferrite and austenite than the hot rolling process.

The specimens were cut,  $15 \times 10 \times 5 \text{ mm}$ , and machined from the as received materials. After this, the specimens were isothermally treated at 800 °C, 850 °C, 900 °C and 950 °C for 5, 15, 30, 45 and 60 minutes followed by water cooling.

The deleterious phase quantification was performed by image analysis of the specimens prepared with electrolytic etching in 15% KOH solution (3V, 12 s). The images were obtained in a light optical microscope with 240X, 475X and 950X magnifications. The quantifications were performed with *Image Tools* software<sup>18</sup> analyzing 20 fields per condition.

The DL-EPR tests were performed to evaluate the degree of sensitization due to the precipitation of deleterious phases. These tests were conducted in 2.00 M  $H_2SO_4$  + 0.01 M KSCN + 0.50 M NaCl solution at room temperature, 40 °C and 60 °C. As reported, this electrolyte had been previously used to study the effects of sigma phase precipitation in duplex stainless steels<sup>12,13</sup>. The tests were conducted in a three electrode cell with working electrode, saturated calomel electrode (SCE) as a reference, and Pt foil as a counter electrode. Working electrodes were constructed with each SDSS sample embedded in epoxy resin with cooper wire as an electric contact. The working electrodes were ground sequentially with 100, 220, 320 and 400 emery papers, degreased with alcohol and cleaned in water. After this, the edges of the samples were protected to avoid crevices. The test was initiated after the open circuit potential ( $E_{oc}$ ) had been achieved, in approximately 30 minutes. The potential was varied in the anodic direction with a sweep rate of  $1.0 \text{ mV.s}^{-1}$  until  $0.3 V_{SCE}$  (in relation with SCE) for all the conditions analyzed. Then, the scan was reversed, maintaining the same sweeping rate in the cathodic direction until it reached the  $E_{oc}$  value again. The degree of sensitization (DOS) was evaluated by two methodologies. The first one was by the  $I_r/I_a$  ratio, where  $I_a$  is the maximal activation peak current of the anodic scan and  $I_r$  is the maximal reactivation peak current observed in the reversed scan. The second method proposed was by the  $Q_f/Q_a$  charges ratio, where  $Q_a$  is the integrated current

**Table 1.** Chemical compositions of the materials studied.

Material	%wt. (%Fe = balance)										
	Cr	Ni	Mo	Mn	Si	N	Cu	W	C	P	S
SD-A	24.57	6.68	3.75	0.83	0.34	0.28	0.25	---	0.02	0.026	0.000
SD-B	24.80	6.75	3.79	0.78	0.54	0.27	0.10	0.04	0.019	0.026	0.001

**Table 2.** Percentages of phases and grain sizes in materials SDA and SDB as received.

Material	Ferrite ( $\delta$ )				Austenite ( $\gamma$ )			
	Amount (%)	Grain size		Amount (%)	Grain size			
		$\mu\text{m}$	ASTM N°		$\mu\text{m}$	ASTM N°		
SD-A	55.05	29.42	7.2	44.95	24.75	7.7		
SD-B	49.95	132.36	2.8	50.05	138.32	2.7		

under the peak over the time in the anodic scan and  $Q_r$  is the integrated current under the peak over the time observed in the reversed scan<sup>19</sup>. The second method was proposed, in this work, because of the appearance of several peaks in the activation and reactivation scans. After the tests, some specimens were observed in the light optical microscope (LOM). For a better characterization, the samples were slightly polished with alumina 0.1  $\mu\text{m}$  in aqueous suspension before examination.

The DL-EPR test was also performed using a portable cell in order to develop it for field application. A small cell was fixed to the specimen surface by cyanoacrylate-based adhesive. After this, hot-melt thermoplastic adhesive was used for reinforcement of the base cell. Finally, after pouring the solution into the cell, a platinum wire counter electrode was carefully screwed around the saturated calomel electrode (SCE) and immersed in the electrolytic cell. Figure 1 shows schematically the cell fixed on the surface of the specimen and the disposition of electrodes for this field analysis.

### 3. Results

DL-EPR tests were performed on the as received materials at room temperature (25 °C), and did not show reactivation peaks. The  $I_r/I_a$  and  $Q_r/Q_a$  values obtained for different conditions of the isothermal treatment are shown in Figures 2 and 3 respectively, with similar behaviour in the SD-A and SD-B steels. In these figures, the dashed line indicates the limit of  $I_r/I_a$  equal to 0.05, as proposed by Lopez et al.<sup>12,13</sup> for DSS tested at 30 °C. In the fine grained SD-A steel, higher reactivation peaks were observed in the specimens aged at 800 °C and 850 °C. In SD-B steel the higher peaks were observed in the specimens aged at 800, 850 and 900 °C, and the intensities were lower than in the SD-A specimens. It can be also be observed that the aging time necessary to reach the limit of  $I_r/I_a = 0.05$  is lower in the SD-A specimens than in SD-B steel specimens. In specimens of the SD-A aged at 850 °C this time was approximately 20 minutes, while in the SD-B specimens aged at 850 and 900 °C this time was approximately 36 minutes. The explanation is that the decrease of grain size enhances the kinetics of precipitation of deleterious phases, i.e. increases the sensitization susceptibility of the alloy. Table 3 summarizes the results of  $I_r/I_a$  and  $Q_r/Q_a$  from Figures 2 and 3.

The DL-EPR test was originally developed to evaluate the intergranular corrosion resistance of austenitic stainless steels (ASS) of type AISI 304, using a solution of 0.5 M  $\text{H}_2\text{SO}_4$  + 0.01 M KSCN at room temperature<sup>13</sup>. For more corrosion resistant materials, more aggressive test solutions and/or higher temperatures must be employed, although the DOS may also be influenced by the sweep rate used. A second set of experiments were performed at 60 °C, however, in these tests reactivation peaks were detected in the as received samples of both materials (Figure 4), which means that the electrolyte was too aggressive. After several experiments it was found that 40 °C was the most suitable temperature for testing the material under these conditions, because the DL-EPR curves showed no reactivation peaks in the as received condition (solution treatment) for both materials. Furthermore, tests performed at several heat treatment conditions showed a higher sensitivity to the

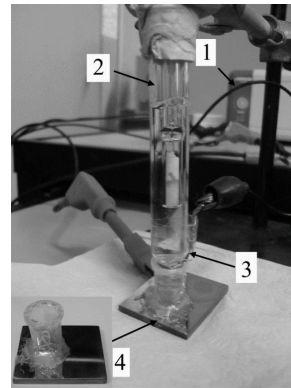


**Figure 1.** Cell for portable and field analysis: 1 – Potentiostat – galvanostat; 2 – Saturated calomel electrode (SCE); 3 – Counter electrode; 4 – Cell fixed on the surface of the specimen.

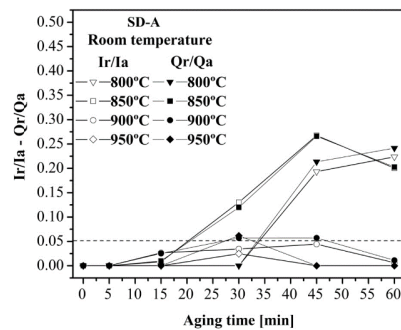


**Figure 2.**  $I_r/I_a$  and  $Q_r/Q_a$  versus aging time for SD-A in 2.00 M  $\text{H}_2\text{SO}_4$  + 0.01 M KSCN + 0.50 M NaCl solution test at room temperature.

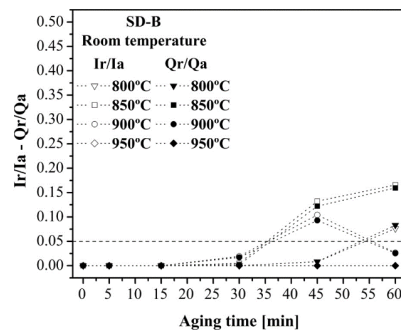


**Figure 3.**  $I_r/I_a$  and  $Q_r/Q_a$  versus aging time for SD-B in 2.00 M  $\text{H}_2\text{SO}_4$  + 0.01 M KSCN + 0.50 M NaCl solution test at room temperature.

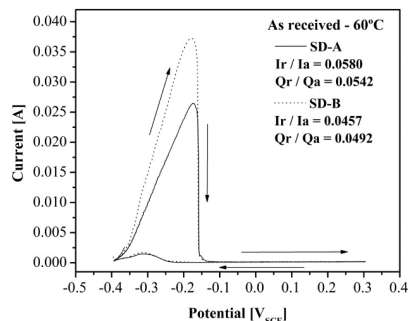


**Figure 4.** DL-EPR curves of un-aged SD-A and SD-B tested at 60 °C in 2.00 M  $\text{H}_2\text{SO}_4$  + 0.01 M KSCN + 0.50 M NaCl solution.

**Table 3.**  $I_r/I_a$  and  $Q_r/Q_a$  values obtained for SD-A and SD-B in 2.00 M  $H_2SO_4$  + 0.01 M KSCN + 0.50 M NaCl solution test at room temperature.

		DOS 2.00 M $H_2SO_4$ + 0.01 M KSCN + 0.50 M NaCl - room temperature							
Material	Aging Time (min)	Aging Temperature (°C)							
		800		850		900		950	
		$I_r/I_a$	$Q_r/Q_a$	$I_r/I_a$	$Q_r/Q_a$	$I_r/I_a$	$Q_r/Q_a$	$I_r/I_a$	$Q_r/Q_a$
SD-A	5	0.000	0.000	0.000	0.000	0.000	0.000	0.000	0.000
	15	0.000	0.000	0.008	0.010	0.027	0.025	0.000	0.000
	30	0.000	0.000	0.130	0.120	0.035	0.057	0.000	0.000
	45	0.193	0.213	0.268	0.266	0.044	0.057	0.025	0.062
	60	0.224	0.242	0.200	0.203	0.006	0.011	0.000	0.000
SD-B	5	0.000	0.000	0.000	0.000	0.000	0.000	0.000	0.000
	15	0.000	0.000	0.000	0.000	0.000	0.000	0.000	0.000
	30	0.000	0.000	0.005	0.002	0.020	0.017	0.000	0.000
	45	0.008	0.008	0.132	0.122	0.104	0.093	0.000	0.000
	60	0.076	0.083	0.166	0.160	0.026	0.025	0.000	0.000

precipitation of deleterious phases than tests performed at room temperature, as shown in Figures 5 and 6. In this test condition the behaviour of the  $I_r/I_a$  and  $Q_r/Q_a$  ratios were very similar, as summarized in Table 4. For this reason only the  $Q_r/Q_a$  ratio versus deleterious phases precipitated are represented in Figures 7 and 8 and Table 5 for SD-A and SD-B. Additionally, as already observed in the tests at room temperature, the tests at 40 °C showed that the increase of  $I_r/I_a$  and  $Q_r/Q_a$  was faster in SD-A than in SD-B, due to its smaller grain size.

Figures 9 and 10 show the microstructures of SD-A aged at 850 °C for 60 minutes and SD-B aged at 850 °C for 45 minutes, respectively. The microstructures were revealed by DL-EPR tests at room temperature and 40 °C. In Figures 9a, 10a and b the arrows indicate the formation of the deleterious phases sigma ( $\sigma$ ) and secondary austenite ( $\gamma_2$ ), which resulted from the eutectoid decomposition of ferrite ( $\delta$ ). The arrows in Figure 9b point the cavities formed in the eutectoid  $\sigma + \gamma_2$  structures during the DL-EPR test.

As shown in a recent work<sup>7</sup>, depending on the conditions of the isothermal treatment, the  $\sigma$  phase may be formed from the  $\delta$  as a result of lamellar eutectoid decomposition, or independently, as large plates. Figure 11 shows the microstructure of SD-B aged at 900 °C for 45 minutes, observed after the DL-EPR test at room temperature. In these images it is possible to observe the formation of  $\sigma$  phase from the decomposition of ferrite into lamellar eutectoid, resulting in numerous sites of low resistance to corrosion.

In the specimens of SD-A and SD-B treated at 850 and 900 °C for long periods of time was observed a reduction in the  $I_r/I_a$  and  $Q_r/Q_a$  values measured by DL-EPR. This phenomenon maybe associated to the formation of thicker  $\sigma$  lamellae, as well as the formation and independent  $\gamma_2$  particles precipitation<sup>7</sup>. Besides, the high temperature and long aging time also promotes the Cr and Mo diffusion, reducing the amount of chromium and molybdenum depleted boundaries, resulting in a lower value of  $I_r/I_a$  and  $Q_r/Q_a$ . This healing process was reported by Angelini et al.<sup>20</sup>.

A clear example of desensitization process is shown by specimens aged at 950 °C, Figures 7 and 8. At this temperature,

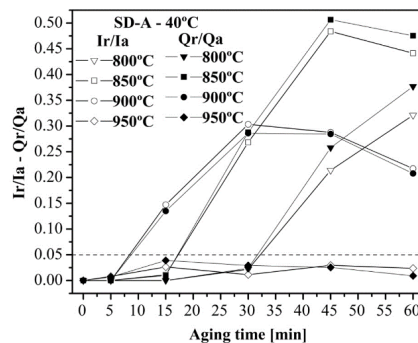


**Figure 5.**  $I_r/I_a$  and  $Q_r/Q_a$  versus aging time for SD-A in 2.00 M  $H_2SO_4$  + 0.01 M KSCN + 0.50 M NaCl solution test at 40 °C.

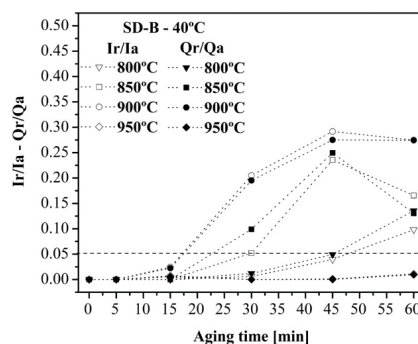


**Figure 6.**  $I_r/I_a$  and  $Q_r/Q_a$  versus aging time for SD-B in 2.00 M  $H_2SO_4$  + 0.01 M KSCN + 0.50 M NaCl solution test at 40 °C.

despite the intense precipitation of deleterious phases in the initial stages of isothermal treatment, the  $Q_r/Q_a$  values remained below the critical value. This maybe a consequence of the  $\gamma_2$  formed independently, and/or the formation of coarse  $\sigma$  phase plates at this high temperature, leading to only a few boundaries with low corrosion resistance. Figure 12 shows the microstructure of the SD-A treated at 950 °C for 45 minutes after DL-EPR test at room temperature, where it is possible

to observe the  $\gamma_2$  plates precipitated independently, as well as large  $\sigma$  plates indicated by arrows. Another arrows point shows regions with low corrosion resistance.

Several reactivation curves showed the presence of two or more peaks and for that reason, measurements of  $Q_r/Q_a$  ratios were performed to verify some influences in the  $I_r/I_a$ , where maximum  $I_r$  and  $I_a$  values were adopted. As shown,

for the different conditions studied, the obtained results were very similar. According to Číhal et al.<sup>21</sup>, the presence of more than one peak is related to different concentrations of chromium depleted zones. Goodwin et al.<sup>22</sup> attributed the second reactivation peak to the sigma phase precipitation in a DSS. In this sense, Wu & Tsai<sup>23</sup> mentioned that in Ni Alloy 600 these peaks are related to pitting corrosion, intergranular

**Table 4.**  $I_r/I_a$  and  $Q_r/Q_a$  values obtained for SD-A and SD-B in 2.00 M  $H_2SO_4$  + 0.01 M KSCN + 0.50 M NaCl solution test at 40 °C.

		DOS							
		2.00 M $H_2SO_4$ + 0.01 M KSCN + 0.50 M NaCl – 40 °C							
Material	Aging Time (min)	Aging Temperature (°C)							
		800		850		900		950	
		$I_r/I_a$	$Q_r/Q_a$	$I_r/I_a$	$Q_r/Q_a$	$I_r/I_a$	$Q_r/Q_a$	$I_r/I_a$	$Q_r/Q_a$
SD-A	5	0.000	0.000	0.000	0.000	0.000	0.000	0.008	0.007
	15	0.000	0.000	0.011	0.010	0.147	0.135	0.026	0.039
	30	0.022	0.024	0.269	0.288	0.303	0.286	0.011	0.029
	45	0.214	0.258	0.484	0.507	0.288	0.285	0.030	0.025
	60	0.321	0.377	0.441	0.475	0.217	0.208	0.024	0.009
SD-B	5	0.000	0.000	0.000	0.000	0.000	0.000	0.000	0.000
	15	0.000	0.000	0.000	0.000	0.025	0.022	0.007	0.006
	30	0.006	0.012	0.052	0.099	0.205	0.195	0.000	0.000
	45	0.040	0.049	0.236	0.249	0.292	0.275	0.001	0.000
	60	0.098	0.136	0.166	0.130	0.274	0.274	0.011	0.009

**Table 5.** Deleterious phases precipitated (DP) percentage and  $Q_r/Q_a$  values obtained for SD-A and SD-B in 2.00 M  $H_2SO_4$  + 0.01 M KSCN + 0.50 M NaCl solution test at 40 °C.

		DP and DOS							
		2.00 M $H_2SO_4$ + 0.01 M KSCN + 0.50 M NaCl – 40 °C							
Material	Aging Time (min)	Aging Temperature (°C)							
		800		850		900		950	
		DP	$Q_r/Q_a$	DP	$Q_r/Q_a$	DP	$Q_r/Q_a$	DP	$Q_r/Q_a$
SD-A	5	4.11	0.000	8.69	0.000	11.91	0.000	11.77	0.007
	15	9.09	0.000	12.06	0.010	16.42	0.135	17.38	0.039
	30	11.31	0.024	24.30	0.288	29.18	0.286	23.51	0.029
	45	18.14	0.258	33.02	0.507	31.97	0.285	26.51	0.025
	60	25.99	0.377	38.03	0.475	35.22	0.208	27.52	0.009
SD-B	5	0.00	0.000	0.00	0.000	1.00	0.000	5.41	0.000
	15	0.83	0.000	3.47	0.000	4.62	0.022	8.70	0.006
	30	1.52	0.012	6.47	0.099	20.41	0.195	16.88	0.000
	45	5.49	0.049	16.59	0.249	33.82	0.275	28.86	0.000
	60	7.75	0.136	31.02	0.130	37.45	0.274	29.73	0.009

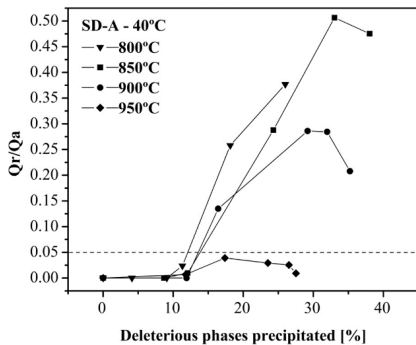


**Figure 7.**  $Q_r/Q_a$  versus deleterious phases for SD-A in 2.00 M  $H_2SO_4$  + 0.01 M KSCN + 0.50 M NaCl solution test at 40 °C.

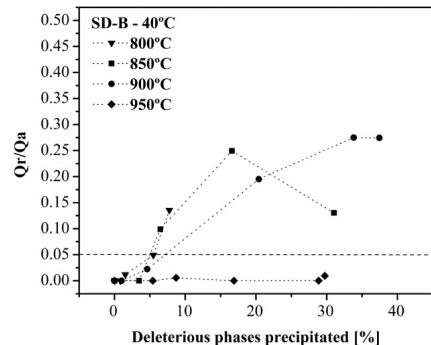


**Figure 8.**  $Q_r/Q_a$  versus deleterious phases for SD-B in 2.00 M  $H_2SO_4$  + 0.01 M KSCN + 0.50 M NaCl solution test at 40 °C.

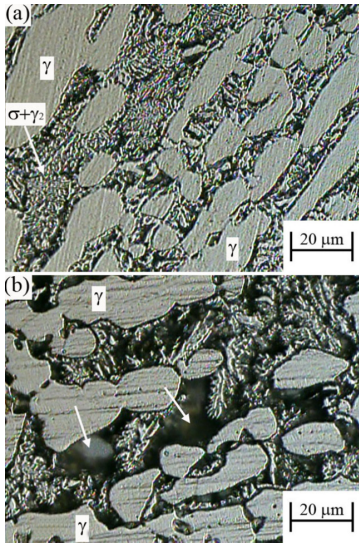


**Figure 9.** Microstructures observed after DL-EPR tests in SD-A aged at 850 °C for 60 min.

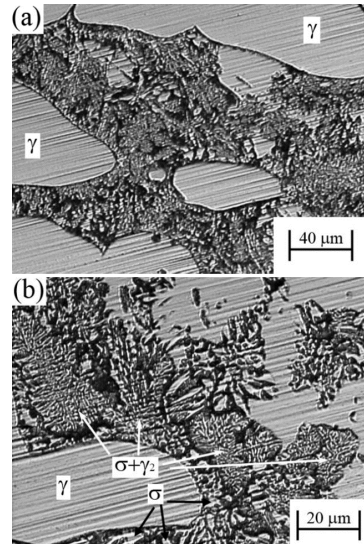


**Figure 11.** SD-B aged at 900 °C for 45 minutes, after DL-EPR test at room temperature.

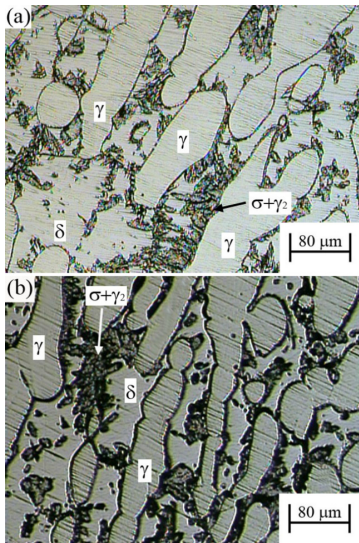


**Figure 10.** Microstructures observed after DL-EPR tests in SD-B aged at 850 °C for 45 min.

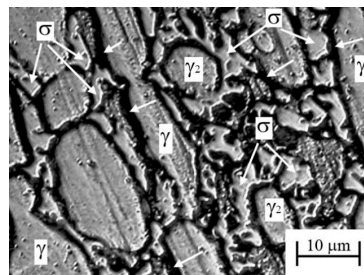


**Figure 12.** SD-A aged at 950 °C for 45 minutes, after DL-EPR test at room temperature.

corrosion and matrix corrosion with the decreasing potential. In this context, Figure 13 shows the DL-EPR cycles where the highest  $I_r/I_a$  and  $Q_r/Q_a$  ratios were obtained, indicating two reactivation peaks at 800 and 850 °C in SD-A and SD-B. The specimens of SD-A and SD-B treated at 800 and 850 °C showed that reactivation curves as two distinct peaks, but this phenomenon tends to disappear in specimens aged at 900 °C. In specimens aged at 950 °C the two reactivation peaks were not so clearly observed, only a small hump could be noted.

DL-EPRs were also tested in a portable cell, as shown in Figure 1, envisaging its use as a field and non-destructive analysis. Two test conditions were performed, in specimens of SD-B aged at 800 °C and 850 °C for 60 minutes. The results were very close to those obtained in the conventional cell, as shows in Figure 14.

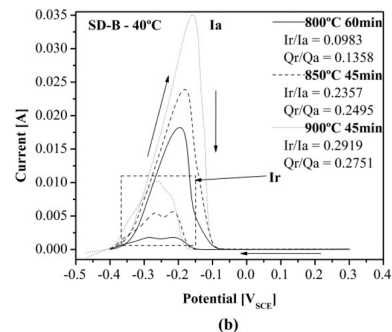
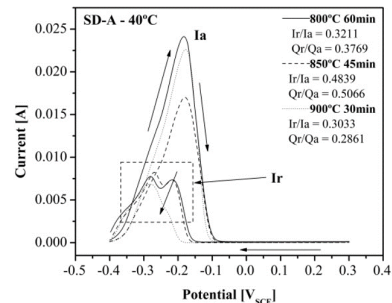


**Figure 13.** DL-EPR cycles of (a) SD-A and (b) SD-B with  $I_r/I_a$  and  $Q_r/Q_a$  ratios. 2.00 M  $H_2SO_4$  + 0.01 M KSCN + 0.50 M NaCl solution test at 40 °C.

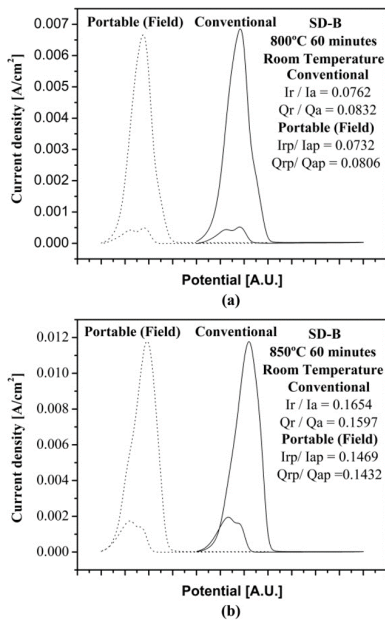


**Figure 14.** Comparison between DL-EPR cycles obtained in a conventional cell and in a portable cell for different aging time for SD-B: (a) 800 °C/60 min.; (b) 850 °C/60 min. 2.00 M H<sub>2</sub>SO<sub>4</sub> + 0.01 M KSCN + 0.50 M NaCl solution test at room temperature.

## 4. Conclusions

In the present study the sensitization of two superduplex steels with similar composition (UNS S32750) but different grain sizes (SD-A-fine grained and SD-B-coarse grained)

## References

- Gunn RN. *Duplex stainless steels: microstructure, properties and applications*. Cambridge: Abington Publishing; 2003.
- Muthupandi V, Bala Srinivasan P, Seshadri SK and Sundaresan S. Effect of weld metal chemistry and heat input on the structure and properties of duplex stainless steel welds. *Materials Science and Engineering A*. 2003; 358(1-2):9-16. [http://dx.doi.org/10.1016/S0921-5093\(03\)00077-7](http://dx.doi.org/10.1016/S0921-5093(03)00077-7).
- Pardal JM, Tavares SSM, Cindra Fonseca MP, Silva MR and Ferreira MLR. Study of deleterious phase precipitation under continuous cooling of superduplex stainless steel UNS S32750. *Materials Science and Technology*. 2012; 28(3):295-302. <http://dx.doi.org/10.1179/1743284711Y.0000000040>.
- Chen TH and Yang JR. Effects of solution treatment and continuous cooling on  $\sigma$ -phase precipitation in a 2205 duplex stainless steel. *Materials Science and Engineering A*. 2001; 311(1-2):28-41. [http://dx.doi.org/10.1016/S0921-5093\(01\)00911-X](http://dx.doi.org/10.1016/S0921-5093(01)00911-X).
- Pardal JM, Tavares SSM, Fonseca MC, Souza JA, Côte RRA and Abreu HFG. Influence of the grain size on deleterious phase precipitation in superduplex stainless steel UNS32750. *Materials Characterization*. 2009; 60(3):165-172. <http://dx.doi.org/10.1016/j.matchar.2008.08.007>.
- Sieurin H and Sandström R. Sigma phase precipitation in duplex stainless steel 2205. *Materials Science and Engineering A*. 2007; 444(1-2):271-276. <http://dx.doi.org/10.1016/j.msea.2006.08.107>.
- Pardal JM, Tavares SSM, Fonseca MPC, Souza JA, Vieira LM and Abreu HFG. Deleterious phases precipitation on

was studied by means of DL-EPR tests and microscopy. The main conclusions are:

The DL-EPR test for both steels analyzed was optimized by the use of an electrolyte of 2.00 M H<sub>2</sub>SO<sub>4</sub> + 0.01 M KSCN + 0.5 M NaCl solution at 40 °C.

Specimens treated at 850 °C and 900 °C for long periods of time showed a decrease of the degree of sensitization. This process of desensitization can be explained by two parallel mechanisms. The first one is related to the formation of thick lamellar of  $\sigma$  and independent  $\gamma_2$  particles precipitation which has higher corrosion resistance than formed by divorced lamellar eutectoid decomposition. The other one is attributed to Cr and Mo diffusion known as healing. These processes were even more evident in specimens aged at 950 °C, whose  $Q_r/Q_a$  values remained below the critical value of 0.05.

The  $I_r/I_a$  and  $Q_r/Q_a$  ratios presented similar behaviour in all conditions studied.

Two reactivation peaks were observed in specimens aged at 800 and 850 °C. These features in the peak reactivation can be attributed to deleterious phases precipitated and/or changes in their morphology that promoted different concentration of chromium depleted zones.

DL-EPR tests can be used as a portable test for field analysis. Due to the difficulty of achieving the test temperature of 40 °C, it is advisable to use a more aggressive electrolyte to obtain results with greater sensitivity.

## Acknowledgements

The authors acknowledge of the Brazilian research agencies (CAPES, FAPERJ and CNPq) for financial support.

- superduplex stainless steel UNS S32750: Characterization by light optical and scanning electron microscopy. *Materials Research*. 2010; 13(3):401-407. <http://dx.doi.org/10.1590/S1516-14392010000300020>.
- Ramirez AJ, Lippold JC and Brandt SD. The relationship between chromium nitride and secondary austenite precipitation in duplex stainless steels. *Metallurgical and Materials Transactions. A, Physical Metallurgy and Materials Science*. 2003; 34(8):1575-1597. <http://dx.doi.org/10.1007/s11661-003-0304-9>.
- Escriba DM, Materna-Morris E, Plaut RL and Padilha AF. Chi-phase precipitation in a duplex stainless steel. *Materials Characterization*. 2009; 60(11):1214-1219. <http://dx.doi.org/10.1016/j.matchar.2009.04.013>.
- Voronenko BI. Austenitic-ferritic stainless steels: a state of the art review. *Metal Science and Heat Treatment*. 1997; 39(10):428-437. <http://dx.doi.org/10.1007/BF02484228>.
- Maehara Y, Ohmori Y, Murayama J, Fujino N and Kunitake T. Effects of alloying elements on  $\sigma$ -phase precipitation in  $\delta$ - $\gamma$  duplex phase stainless steels. *Metal Science*. 1983; 17(11):541-548. <http://dx.doi.org/10.1179/030634583790420457>.
- Lopez N, Cid M, Puiggali M, Azkarate I and Pelayo A. Application of double loop electrochemical potentiodynamic reactivation test to austenitic and duplex stainless steels. *Materials Science and Engineering A*. 1997; 229(1-2):123-128. [http://dx.doi.org/10.1016/S0921-5093\(97\)00008-7](http://dx.doi.org/10.1016/S0921-5093(97)00008-7).
- Lopez N, Cid M and Puiggali M. Influence of  $\sigma$ -phase on mechanical properties and corrosion resistance of duplex

- stainless steel. *Corrosion Science*. 1999; 41(8):1615-1631. [http://dx.doi.org/10.1016/S0010-938X\(99\)00009-8](http://dx.doi.org/10.1016/S0010-938X(99)00009-8).
14. Amadou T, Sidhom H and Braham C. Double loop electrochemical potentiokinetic reactivation test optimization in checking of duplex stainless steel intergranular corrosion susceptibility. *Metallurgical and Materials Transactions. A, Physical Metallurgy and Materials Science*. 2004; 35(11):3499-3513. <http://dx.doi.org/10.1007/s11661-004-0187-4>.
  15. Deng B, Jiang Y, Xu J, Sun T, Gao J, Zhang L, et al. Application of the modified electrochemical potentiodynamic reactivation method to detect susceptibility to intergranular corrosion of a newly developed lean duplex stainless steel LDX2101. *Corrosion Science*. 2010; 52(3):969-977. <http://dx.doi.org/10.1016/j.corsci.2009.11.020>.
  16. Hong J, Han D, Tan H, Li J, Jiang Y, Deng B, et al. Evaluation of aged duplex stainless steel UNS S32750 susceptibility to intergranular corrosion by optimized double loop electrochemical potentiokinetic reactivation method. *Corrosion Science*. 2013; 68:249-255. <http://dx.doi.org/10.1016/j.corsci.2012.11.024>.
  17. Yang Y, Yan B, Li J and Wang J. The effect of large heat input on the microstructure and corrosion behavior of simulated heat affected zone in 2205 duplex stainless steel. *Corrosion Science*. 2011; 53(11):3756-3763. <http://dx.doi.org/10.1016/j.corsci.2011.07.022>.
  18. University of Texas Health Science Center - UTHSCSA. Department of Dental Diagnostic Science. *Image Tool Version 3.0*. San Antonio, Texas. Available from: <<http://compdent.uthscsa.edu/dig/itdesc.html>>. Access in: 12/12/2014.
  19. British Standards Institution - BSI. *BS EN ISO 12732: corrosion of metals and alloys: electrochemical potentiokinetic reactivation measurement using the double loop method (based on Číhal's method)*. London; 2008.
  20. Angelini E, De Benedetti B and Rosalbino F. Microstructural evolution and localized corrosion resistance of an aged superduplex stainless steel. *Corrosion Science*. 1999; 55(6):1351-1367.
  21. Číhal V, Lasek S, Blahetová M, Kalabisová E and Krhutová Z. Trends in the Electrochemical Polarization Potentiodynamic Reactivation Method – EPR. *Chemical and Biochemical Engineering Quarterly*. 2007; 21:47-54.
  22. Goodwin SJ, Quayle B and Noble FW. Polarization behavior of austenitic and duplex stainless steels in the double loop reactivation test. *Corrosion*. 1987; 43(12):743-747. <http://dx.doi.org/10.5006/1.3583863>.
  23. Wu TF and Tsai WT. Effect of KSCN and its concentration on the reactivation behavior of sensitized alloy 600 in sulfuric acid solution. *Corrosion Science*. 2003; 45(2):267-280. [http://dx.doi.org/10.1016/S0010-938X\(02\)00100-2](http://dx.doi.org/10.1016/S0010-938X(02)00100-2).